


Observation of excitonic series in monolayer and few-layer black phosphorusRuijuan Tian,¹ Ruixiang Fei^{2,*}, Siqi Hu,¹ Tianshu Li,³ Binjie Zheng,⁴ Yi Shi,⁴ Jianlin Zhao,¹ Lijun Zhang,³
Xuetao Gan^{1,†} and Xiaomu Wang^{4,‡}¹*MOE Key Laboratory of Material Physics and Chemistry under Extraordinary Conditions,
and Shaanxi Key Laboratory of Optical Information Technology, School of Physical Science and Technology,
Northwestern Polytechnical University, Xi'an 710129, China*²*Department of Physics, Washington University, St. Louis, Missouri 63130, USA*³*College of Materials Science and Engineering and Key Laboratory of Automobile Materials of MOE,
Jilin University, Changchun 130012, China*⁴*School of Electronic Science and Engineering, Nanjing University, Nanjing 210093, China* (Received 16 July 2019; revised manuscript received 6 May 2020; accepted 8 May 2020; published 3 June 2020)

We report the full sequence of excitonic states in monolayer and few-layer black phosphorus (BP). High-quality BP samples are acquired by treating the silicon oxide substrate with a self-assembled monolayer hydrophobic molecule, which facilitates the access to their ground and higher-lying states of intrinsic excitons through the reflection and photoluminescence excitation spectra. Combined with first-principles and model calculations, we further determine that the exciton binding energy shrinks by ~ 6 -fold from 940 meV in monolayer to 160 meV in bilayer BP, yet it only decreases slightly to 108 meV in trilayer. This could be attributed to the strong interlayer coupling and lattice shrinking in multilayer BP samples. Our results shed light on the unique excitonic optical properties of two-dimensional BP.

DOI: [10.1103/PhysRevB.101.235407](https://doi.org/10.1103/PhysRevB.101.235407)**I. INTRODUCTION**

Two-dimensional (2D) materials have been widely investigated by the scientific community in recent years, due to a large variety of physical properties and novel applications [1–16]. Black phosphorus (BP) has renewed research interest due to its various physical properties and applicabilities in electronic and optoelectronic devices [17,18]. Remarkably, BP has a widely layer-tunable direct band gap varying from 0.3 to 2.0 eV [3,15,19,20]. Its puckered hexagonal structure results in unique anisotropic properties and lone pairs, in terms of orientation-dependent electronic/optical properties and strong van der Waals coupling [2,3,7,8,15,18,21]. In monolayer (also known as phosphorene) and few-layer BP, these anisotropy and interlayer couplings are essential to study unique many-body interactions, manifesting especially in the intriguing excitonic effect. An exciton, bounded together in an electron-hole pair, is produced by light excitation. Accordingly, much effort has been directed toward using BP's optical responses to exploit its fascinating excitonic effects [2,3,7,15,20,22–25]. However, due to the unclear excitonic signatures, a reliable and in-depth understanding of excitons in monolayer and few-layer BP is still largely ambiguous and highly desired.

At present, it is still a challenge to fabricate high-quality few-layer BP, which impedes efforts to understand anisotropic

many-body effects and to discover optoelectronic applications. The unfavorable sample quality can be understood by examining the excitonic emission linewidth. Generally, an intrinsic exciton can exhibit extremely narrow spectral features, e.g., ~ 5 meV for GaN [26] and ~ 5.4 meV for monolayer WSe₂ in experiments at 10 K [27]. Unfortunately, BP samples always present wide emission peaks (>100 meV), even with careful surface protection and environmental control [28].

In this work, we start with the idea of treating a silicon oxide substrate with a self-assembled monolayer hydrophobic molecule to acquire the high-quality monolayer and few-layer BP, and we study experimentally their ground and higher-lying states of intrinsic excitons. With the high-quality samples, we could easily access the fine structure of intrinsic exciton states in monolayer and few-layer BP through reflection and photoluminescence excitation (PLE) spectra, which feature slow scaling for different quantum numbers due to anisotropic in-plane Coulomb screening. We extract the exciton binding energies combined with first-principles and model calculations, which characterize the anomalous scale for BP with different layers. This could be attributed to the strong interlayer coupling and lattice shrinking in multilayer samples.

II. HIGH-QUALITY BP SAMPLES

The key point to realize a high-quality BP sample is choosing a proper substrate to significantly improve the sample/substrate interface in addition to only protecting the top surface of BP. A silicon substrate covered with a ~ 280 -nm-thick silicon oxide (SiO₂/Si) is normally utilized as the substrate for studying atomically layered materials leveraging the clear optical contrast. Unfortunately, SiO₂/Si is hydrophilic

*Present address: Department of Chemistry, University of Pennsylvania, Philadelphia, PA 19104-6323, USA.

†Author to whom all correspondence should be addressed: xuetaogan@nwpu.edu.cn‡xiaomu.wang@nju.edu.cn

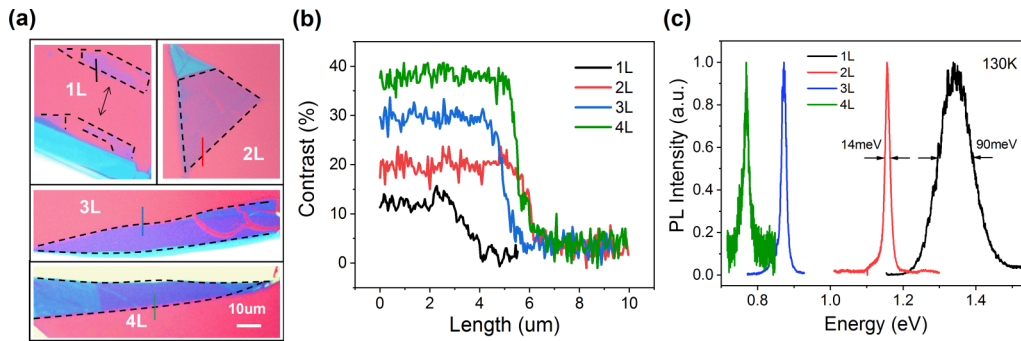


FIG. 1. High-quality few-layer BP samples. (a) Optical micrograph of monolayer to quadralayer BP samples on OTS-modified substrates. The micrographs were captured by a CCD camera coupled with a microscope. The number of layers is determined by the optical contrasts in the red channel of the CCD images. (b) Optical contrast profiles in the red channel of the CCD images along with the solid lines marked in (a). The contrast difference between adjacent atomic layers is around 7.2%. (c) PL spectra of monolayer to quadralayer BP samples. The number of layers is further verified through the peak positions of PL spectra. High-quality BP samples are confirmed by the narrow linewidths of PL emission peaks.

with the richness of hydroxy and dangling bonds. This microscopic atmosphere is prone to prompt the formation and dissolution of phosphoric oxides, which will lead to significant degradation of BP layers. Accordingly, we propose modifying the hydrophilicity of the substrate as an appropriate idea to improve BP sample quality. To verify this idea, we modified a SiO_2/Si substrate by hydrophobic self-assembled monolayer (SAM) octadecyltrichlorolane (OTS, $\text{C}_{18}\text{H}_{37}\text{Cl}_3\text{Si}$), as schematically shown in Fig. S1(a) (see the Supplemental Material for details [29]). The fabrication process and the surface morphology of the OTS SAM were demonstrated in our previous work [30], which has better flatness than the bare SiO_2/Si substrate. It could improve the high quality of BP samples significantly. Monolayer and few-layer BP was prepared by standard mechanical exfoliation from the bulk BP crystal (HQ Graphene Inc.) on the polydimethylsiloxane (PDMS) and transferred to the modified substrate. After that, samples were loaded into a chamber [Montana Instruments Crystation (4200-520)] with a slow flow of nitrogen gas to prevent degradation. Optical microscope images of monolayer to quadralayer BP on the OTS-modified substrates are shown in Fig. 1(a).

The number of layers of these BP samples is determined from the optical contrasts in the red channel of microscope images shown in Fig. 1(b). As reported by Li *et al.* [15], with each additional atomic layer the optical contrast in the red channel of a colored charge-coupled-device (CCD) camera increases by around 7% in few-layer BP. Figure 1(b) displays the optical contrasts obtained along the corresponding colored solid lines in Fig. 1(a) for monolayer to quadralayer BP samples. The optical contrasts are uniformly increased by around 7% with the increased number of layers. Although other microscope techniques with even higher accuracy are desired, such as atomically high-resolution scanning transmission electron microscopy (HR-STEM) and atomic-force microscopy (AFM), BP is very unstable in ambient conditions with the exposure of oxygen, moisture, and optical light, hindering these measurements on thin BP samples. Thanks to the moderately thick layer of trilayer BP, its height of 3.8 nm is estimated by AFM, as shown in Figs. S3(c) and S3(d) of the Supplemental Material [29]. By considering

the interlayer distance of 0.55 nm measured by HR-STEM (see Fig. S11 in the Supplemental Material [29]), the layer number is calculated as 3 with an average height of ~ 0.74 nm in monolayer BP. The number of layers is further verified through PL spectroscopy. Figure 1(c) shows the PL spectra of these BP samples. The peak energy decreases continuously with increasing layer number: 1.34 ± 0.04 eV for monolayer, 1.16 ± 0.02 eV for bilayer, 0.87 ± 0.01 eV for trilayer, and 0.77 ± 0.01 eV for quadralayer. The energy levels of these ground exciton states of few-layer BP are consistent with the results reported in Ref. [15] (detailed comparisons are shown in Table I of the Supplemental Material [29]).

As we expected, the PL spectra of BP samples exhibit surprisingly sharp and intense features on the OTS-modified substrate, as shown in Fig. 1(c). The PL peaks are with linewidths [with a full width at half-maximum (FWHM) of ~ 15 meV for bilayer, trilayer, and quadralayer at 130 K] that are narrower than those in previous reports, which are around 100 meV for few-layer BP [15,25]. To further verify the improvement effect by the OTS layer, we carry out control experiments by measuring PL spectra of few-layer BP samples on bare SiO_2/Si substrate, which displays a much broader peak linewidth than those on OTS-modified SiO_2/Si , as shown in Fig. S1(b) of the Supplemental Material [29]. Two bilayer BP samples are transferred to the bare SiO_2/Si and the OTS-modified SiO_2/Si separately. The FWHM of the sample on the OTS-modified substrate is at least sevenfold narrower than that on the bare SiO_2/Si substrate.

In addition, in the previously reported observations of BP excitons, there are distinct Stokes shifts (~ 1.5 meV [31], ~ 19 meV [32], and 610 meV [33]) obtained by comparing the energies of PL emission peaks and optical absorption peaks of BP samples. The origin of this Stokes shift is the nonradiative channel via the interface between BP and SiO_2/Si substrate [34]. In our experiments, we also measure the absorption peaks of the BP samples, which are extracted by the differential reflection spectra from the OTS-modified substrate with and without BP samples ($\Delta R/R$). Figures 2(a)–2(c) plot the absorption spectra from monolayer to trilayer BP on the OTS-modified substrate as well as the PL spectra. Tiny Stokes shifts (< 1 meV) are observed for these samples, indicating

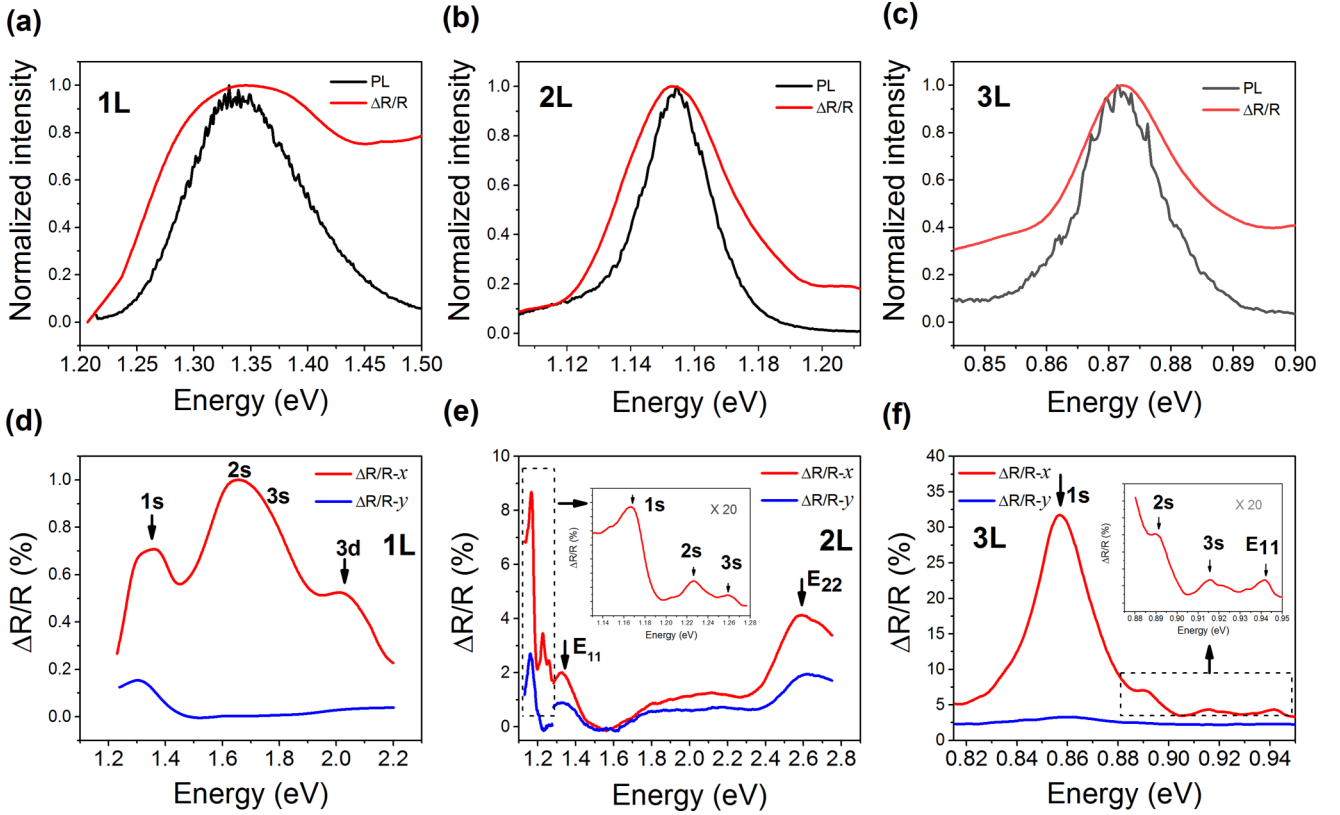


FIG. 2. PL and differential reflection spectra of monolayer to trilayer BP. (a)–(c) PL and differential reflection spectra of ground excitonic state of monolayer (a), bilayer (b), and trilayer (c) BP samples, showing tiny energy shifts between the peaks of PL emission and differential reflection peak. (d)–(f) Differential reflection spectra of excitonic states of monolayer (d), bilayer (e), and trilayer (f) BP samples with the illumination light polarized along the armchair (x) and zigzag (y) directions of the BP structure. The arrows indicate the ($1s$, $2s$, $3s$, ...) excitonic series.

less phonon emission involved in the exciton emission of BP samples. This further confirms the intrinsic exciton behavior in our high-quality few-layer BP samples.

III. FINE STRUCTURE OF AN INTRINSIC EXCITON

While many theoretical efforts have been committed to studying the exciton binding energy and the excitonic state series of BP, the predicted series are not confirmed in experiments [24,35,36]. Here, the significantly improved quality of BP samples on the OTS-modified substrate provides an opportunity to investigate the intrinsic properties and fine structure of excitons in few-layer BP. To acquire precise exciton binding energy, we study the excitonic series for monolayer and few-layer BP. The excitonic series are denoted in analogy to the hydrogen spectral series as $1s$, $2s$, $3s$, and so on, which are the ground and excited states of excitons.

In previous works, only the first “bright” state of the excitonic series in few-layer BP was observed [7,15]. However, for the excited-state excitons, namely the signature of high-quantum-number transitions, it is difficult to distinguish them for the poor samples. If the quality of the BP sample is poor, these high-order transitions are concealed not only by their relative weakness but also by the wide spectrum of the ground-state exciton. In our experiment, these difficulties could be overcome by the acquisition of a high-quality

BP sample, as mentioned above. Figures 2(d)–2(f) show the differential reflection spectra measured with the illumination light polarized along with the two characteristic directions (armchair and zigzag edges of BP crystal) of monolayer, bilayer, and trilayer BP. In addition to the prominent ground excitonic state (which is located at the energy of the PL emission peak and labeled as $1s$), we also observe multiple additional peaks on the high-energy side of the main transition. The energy spacing as well as the intensity decreases for the first few peaks, presenting characteristic features of excitonic series. We accordingly assign these peaks as excitonic series with the labels of $2s$, $3s$, and $3d$ for monolayer, and $2s$ and $3s$ for bilayer and trilayer, respectively, as shown in Figs. 2(d)–2(f). In contrast, the energy spacings and intensities increase again for the last one or two peaks, which are assigned as the higher-order intersubband transitions.

It should be noted that these high-quantum-number excitonic states are very reliable in our high-quality BP samples. We identify several samples and multiple measurements to avoid the noise and interference effect. These fine-structured spectra are consistently observed. They also have the same anisotropic linear polarization dependence as the PL emission (see Figs. S6 and S7 in the Supplemental Material [29]). Remarkably, these exciton signatures are directly distinguishable in the reflection spectrum, while for transition-metal

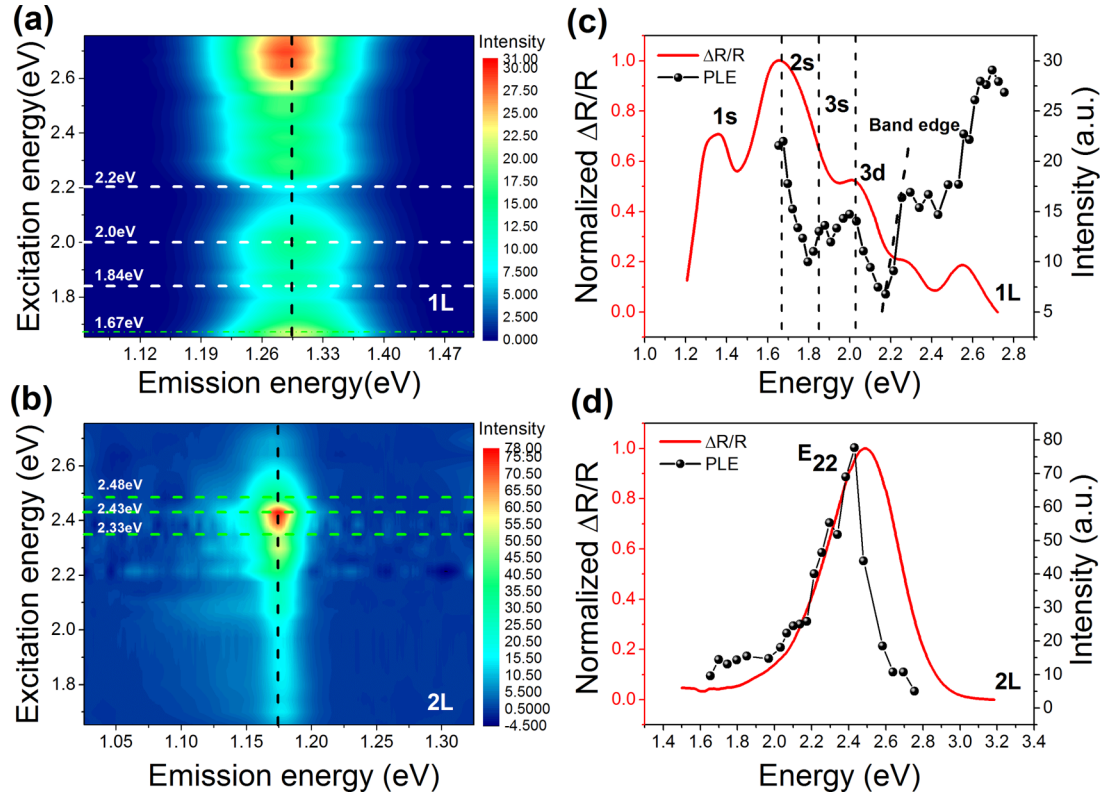


FIG. 3. PLE spectra of monolayer and bilayer BP. (a), (b) PLE intensity maps as a function of both excitation and emission photon energies for monolayer (a) and bilayer (b). (c), (d) PL intensity (right axis) at the emission peak of the monolayer (a) and bilayer (b) BP as a function of excitation photon energies. The differential reflection spectra (left axis) are also superimposed for comparison.

dichalcogenide monolayers, such as MoS₂ and WS₂, they can only be identified in the derivative of the differential reflection spectra.

We further verify these features by examining the photoluminescence excitation (PLE) spectra in monolayer and few-layer BP. Figures 3(a) and 3(b) present a two-dimensional plot of PLE spectra as a function of both excitation and emission photon energies for monolayer and bilayer BP, which are excited by lasers polarized along with the armchair direction of BP crystal. Excited by laser with different photon energies, the PL spectra exhibit similar shapes but with different emission intensities, as detailed in Fig. S8 of the Supplemental Material [29]. The PL peak intensities as a function of excitation energies [which are the spectra taken along the dashed vertical lines in Figs. 3(a) and 3(b)], together with reflection spectra, are both plotted in Figs. 3(c) and 3(d) for monolayer and bilayer BP. We find that the PLE spectra perfectly match the optical reflection spectra. In particular, the PLE of monolayer BP accurately reproduces all the fine features obtained in the differential reflection spectrum, while in the case of bilayer BP, the PLE cannot approach the excitonic states due to the instrument limitation, and it also agrees well with the E_{22} transition in the differential reflection spectrum.

With the information about exciton spectra, we can extract the binding energies and quasiparticle band gaps in a comparably reliable manner. In the monolayer or few-layer BP, the exciton energies exhibit a much weaker scaling with the quantum number in comparison with the other 2D materials. Such an anomalous exciton state evolution is embodied in

the energy separations between bright exciton states. For example, as shown in Figs. 2(d) and 3(c), the energy difference between $1s$ and $2s$ (Δ_{12}) is 320 meV while the energy difference between $2s$ and $3s$ (Δ_{23}) is 120 meV in monolayer BP. Such a feature is also observed in bilayer and trilayer BP, e.g., $\Delta_{12} = 60$ meV and $\Delta_{23} = 33$ meV for bilayer, and $\Delta_{12} = 35$ meV and $\Delta_{23} = 24$ meV for trilayer. In addition, the exciton binding energy, defined by the energy difference between the first bright exciton and the quasiparticle band gap, exhibits an unusual scaling with the layer number. The exciton binding energy shrinks by ~ 6 -fold from 940 meV in the monolayer to 160 meV in bilayer BP, yet it only decreases slightly to 108 meV in trilayer BP. Here, the exciton binding energy in monolayer BP of 940 meV is consistent with our previous work [7].

IV. ANISOTROPIC SCREENING AND EFFECTIVE-MASS MODEL

The isotropic effective-mass model in the 2D quantum-confined system has been widely applied to explain the exciton binding energy and series of 2D semiconductors such as BN and transition-metal dichalcogenides (TMDs) [4,16]. The predicted binding energy and exciton series nicely match the experimental observations [4,9]. Such good agreement can be understood because of the highly symmetric in-plane lattice of the above-discussed 2D semiconductors, e.g., the threefold rotational symmetry for MoS₂.

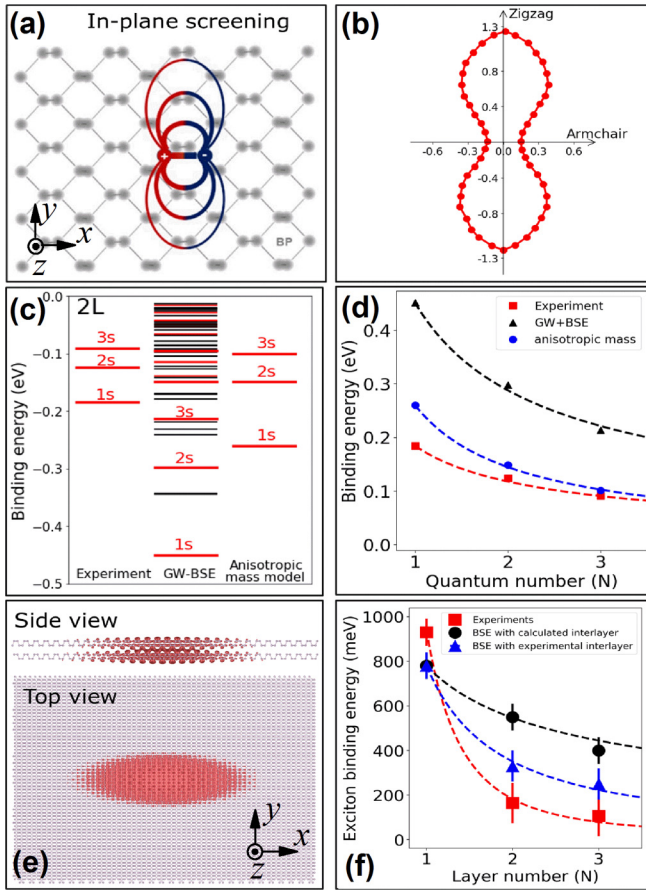


FIG. 4. Theoretical calculation of excitonic states of BP. (a) Schematic of in-plane anisotropic Coulomb screening of excitonic states in 2D BP. (b) Highly anisotropic effective mass of electron for 2D BP. (c) Binding-energy spectrum of the excitonic series of the bilayer BP. Left panel: experimental results. Middle panel: GW+BSE calculation results. Right panel: calculation results of anisotropic effective-mass model [12,39]. Bright states are in red and dark states are in black. (d) Scaling law for the exciton states with different quantum numbers for bilayer BP. The power-law fitting curves are presented by dashed lines. (e) Exciton wave function in real space of first bright state, i.e., the 1s state, for bilayer BP. The hole is fixed at the center. (f) Exciton binding energy as a function of BP layer number, showing experimental measured binding energies, BSE-simulated binding energies with the calculated interlayer distance, and BSE-simulated binding energies with the experimentally extracted interlayer distance. x , y , and z denote armchair, zigzag, and out-of-plane orientations, respectively.

However, the isotropic effective-mass model is inapplicable for few-layer BP due to the strong in-plane anisotropic structure. This can be understood from the schematic model shown in Figs. 4(a) and 4(b). The puckered monolayer and few-layer BP only have twofold rotational symmetry, resulting in anisotropic intralayer screened Coulomb interaction. That is, the electronic interaction along the zigzag (y) direction is different from that along the armchair (x) direction, as illustrated in Fig. 4(a). As a result, the equivalent permittivity (ϵ_{eff}) of BP that describes the Coulomb screening in the Hamiltonian should be directionally dependent rather than a constant or spherically symmetric function. Such an

anisotropic interaction is confirmed by the calculations using the random phase approximation (RPA) even in the static limit [37]. On the other hand, Fig. 4(b) shows the electron effective mass from the first-principles simulation, which directly demonstrates the invalidity of the isotropic effective-mass model. This anisotropic band can lead to strong anisotropic collective electronic excitations [38] and anisotropic bounded excitons [39–41].

The anisotropic effective-mass model has been applied to this puckered structure in many references, and the exciton Hamiltonian based on the atomic Rydberg units is [39]

$$H = -\frac{1}{\mu_x} \frac{\partial^2}{\partial x^2} - \frac{1}{\mu_y} \frac{\partial^2}{\partial y^2} + V_{2d}(r), \quad (1)$$

where μ_x and μ_y are the reduced effective masses in the armchair (x) and zigzag (y) directions, respectively. The Rytova-Keldysh-type screening potential is widely used, and the atomic Rydberg unit form reads [12,39,41,42]

$$V_{2d}(r) = -\frac{\pi}{\bar{\epsilon} r_0} \left[H_0\left(\frac{r}{r_0}\right) - Y_0\left(\frac{r}{r_0}\right) \right], \quad (2)$$

where $r_0 = l\epsilon/(\epsilon_1 + \epsilon_2)$ and $\bar{\epsilon} = (\epsilon_1 + \epsilon_2)/2$. Here, l is the thickness of the few-layer BP, ϵ is its bulk dielectric constant, and ϵ_1 and ϵ_2 are the dielectric constants of the surrounding media. It is worthwhile to mention that this effective-mass model is based on the isotropic dielectric constant, so it cannot capture the whole picture of exciton binding energy in the anisotropic BP, especially for the exciton series feature. On the other hand, as shown in Fig. 4(b), the effective mass is described by an approximate “8” shape rather than an ellipse, which is not considered in this anisotropic effective-mass model. Thus, to calculate the excitonic series, we use the density-functional theory plus the GW-BSE many-body theory calculation [43–48] (see the computational details in the Supplemental Material [29]).

V. SLOW SCALING FOR DIFFERENT QUANTUM NUMBERS

Figures 4(c) and 4(d) show the comparison between simulation results and experiment results. Here, we do not consider the substrate screening effect in the GW-BSE calculations due to the computational limitation for the heterostructure. As a result, the binding energy is higher than the experimental results in bilayer BP, which has been discussed by Qiu *et al.* [49]. It is worthwhile to notice that the GW-BSE calculations can elucidate the observed highly nonhydrogenic excitonic series if we use the normalized binding energy (see the Supplemental Material [29]). To further illustrate that, as shown in Fig. 4(d), we fit the exciton binding energy to the form $E_b = \frac{E_b(1s)}{n^\alpha}$, where n is the quantum number, and $E_b(1s)$ is the binding energy of the first bright exciton. We found that the experimental exciton series follows the $1/n^{0.63}$ power law (red dashed line). This power law is different from the $1/n^{0.85}$ power law of the effective-mass model (blue dashed line) but very close to the $1/n^{0.65}$ power law of GW-BSE simulations (black dashed line). Although the substrate screening is neglected in the GW-BSE simulation, the anisotropic dynamic screening and the complicated band

features have been captured in the first-principles simulation, leading to a more accurate power law.

We also plot the wave function of bilayer BP's $1s$ state in real space to characterize the anisotropic feature of BP excitons, as shown in Fig. 4(e). In real space, the excitons are significantly compressed along the y -direction, which is very similar to the monolayer case and has been attributed to the flat band along the zigzag direction. This striped distribution naturally results in one-dimension-like excitonic effects. Because of this, the binding energy scaling in excitonic series for BP is much slower than that in TMDs [4,9].

VI. ANOMALOUS SCALING FOR DIFFERENT LAYERS

As discussed above, the exciton binding energy exhibits an unusual scaling with the layer-number N . We fit the exciton binding energy to the following form:

$$E_b(1s) = \frac{A}{N^\beta} + B. \quad (3)$$

For experimental results, the fitting parameters are $A = 2.5$, $B = 20$ meV, and $\beta = 2.5$. Surprisingly, the power β is much larger than the theoretical simulation, in which $\beta = 0.53$ [black dashed line in Fig. 4(f)]. Even with consideration of the substrate screening effect, the anisotropic model still cannot explain the sharp decrease of exciton binding energy due to the similar dielectric constant of surrounding media for different layers. Unlike other weakly coupled layer structures, few-layer BP has a strong van der Waals interaction, which can be reflected by the interlayer distance-dependent band gap. Here we use experimentally extracted interlayer distance to gauge the van der Waals interaction (see Fig. S11 in the Supplemental Material [29]). As shown by the blue dashed line in Fig. 4(f), the binding energy for bilayer and trilayer BP is closer to the experimental value. Since the experimental interlayer distance is larger than the calculated one without van der Waals interaction, the quantum confinement is weaker.

In addition, such interlayer interaction induces the relaxed shrinks of the lattice structure for a few-layer BP. The lattice constant along the armchair direction (the puckered orientation) in bilayer BP reduces by 1.2% compared with its

monolayer counterpart. This lattice shrink effect along the armchair direction decreases not only the quasiparticle gap [50,51] but also the anisotropic in-plane Coulomb screening, resulting in a weaker excitonic effect. In such a case, the exciton binding energy of bilayer BP should be smaller than that when only the quantum confinement effect is considered.

VII. CONCLUSION

In conclusion, we have obtained high-quality monolayer and few-layer BP samples by substrate modification, which enables us to observe the full sequence of intrinsic exciton states. These excitonic series exhibit highly nonhydrogenic features due to the anisotropic in-plane Coulomb screening in BP. Combined with first-principles and model calculation, we identify the exciton binding energies of BP with different layer numbers. We find a sharp transition from the high-binding-energy phase (monolayer) to the low-binding-energy phase (multilayer) resulting from strong interlayer coupling and lattice shrinking in multilayer samples. Our results present convincing experiment evidence of intrinsic excitonic properties of BP. This in-depth understanding of light-matter interactions also exemplifies monolayer and few-layer BP as a unique platform to study anisotropic and strong many-body physics.

ACKNOWLEDGMENTS

We thank Lang Jiang from Institute of Chemistry, CAS for helping prepare OTS modified substrates. This project was primarily supported by the National Key R&D Program of China (2018YFA0307200 and 2017YFA0303800), the National Natural Science Foundation of China (61775092, 61522507, 61775183, and 11634010), the Fundamental Research Funds for the Central Universities (3102017jc01001 and 3102018jcc034), Program for high-level Entrepreneurial and Innovative Talent Introduction, Jiangsu Province, and the Collaborative Innovation Centre of Advanced Microstructures, Analytical & Testing Center of NPU. The data that support the findings of this study are available from the corresponding author upon reasonable request.

R.T. and R.F. contributed equally to this work.

-
- [1] Q. H. Wang, K. Kalantar-Zadeh, A. Kis, J. N. Coleman, and M. S. Strano, *Nat. Nanotechnol.* **7**, 699 (2012).
 - [2] F. Xia, H. Wang, and Y. Jia, *Nat. Commun.* **5**, 4458 (2014).
 - [3] V. Tran, R. Soklaski, Y. Liang, and L. Yang, *Phys. Rev. B* **89**, 235319 (2014).
 - [4] A. Chernikov, T. C. Berkelbach, H. M. Hill, A. Rigosi, Y. Li, O. B. Aslan, D. R. Reichman, M. S. Hybertsen, and T. F. Heinz, *Phys. Rev. Lett.* **113**, 076802 (2014).
 - [5] M. M. Ugeda, A. J. Bradley, S. F. Shi, F. H. da Jornada, Y. Zhang, D. Y. Qiu, W. Ruan, S. K. Mo, Z. Hussain, Z. X. Shen, F. Wang, S. G. Louie, and M. F. Crommie, *Nat. Mater.* **13**, 1091 (2014).
 - [6] H. Liu, A. T. Neal, Z. Zhu, Z. Luo, X. Xu, D. Tománek, and P. D. Ye, *ACS Nano* **8**, 4033 (2014).
 - [7] X. Wang, A. M. Jones, K. L. Seyler, V. Tran, Y. Jia, H. Zhao, H. Wang, L. Yang, X. Xu, and F. Xia, *Nat. Nanotechnol.* **10**, 517 (2015).
 - [8] V. Tran, R. Fei, and L. Yang, *2D Mater.* **2**, 044014 (2015).
 - [9] H. M. Hill, A. F. Rigosi, C. Roquelet, A. Chernikov, T. C. Berkelbach, D. R. Reichman, M. S. Hybertsen, L. E. Brus, and T. F. Heinz, *Nano Lett.* **15**, 2992 (2015).
 - [10] P. Rivera, J. R. Schaibley, A. M. Jones, J. S. Ross, S. Wu, G. Aivazian, P. Klement, K. Seyler, G. Clark, N. J. Ghimire, J. Yan, D. G. Mandrus, W. Yao, and X. Xu, *Nat. Commun.* **6**, 6242 (2015).
 - [11] J. Yang, T. Lü, Y. W. Myint, J. Pei, D. Macdonald, J.-C. Zheng, and Y. Lu, *ACS Nano* **9**, 6603 (2015).
 - [12] E. Prada, J. V. Alvarez, K. L. Narasimha-Acharya, F. J. Bailen, and J. J. Palacios, *Phys. Rev. B* **91**, 245421 (2015).
 - [13] A. Chernikov, C. Ruppert, H. M. Hill, A. F. Rigosi, and T. F. Heinz, *Nat. Photon.* **9**, 466 (2015).
 - [14] Y. You, X.-X. Zhang, T. C. Berkelbach, M. S. Hybertsen, D. R. Reichman, and T. F. Heinz, *Nat. Phys.* **11**, 477 (2015).

- [15] L. Li, J. Kim, C. Jin, G. J. Ye, D. Y. Qiu, F. H. da Jornada, Z. Shi, L. Chen, Z. Zhang, F. Yang, K. Watanabe, T. Taniguchi, W. Ren, S. G. Louie, X. H. Chen, Y. Zhang, and F. Wang, *Nat. Nanotechnol.* **12**, 21 (2017).
- [16] Z. Jiang, Z. Liu, Y. Li, and W. Duan, *Phys. Rev. Lett.* **118**, 266401 (2017).
- [17] L. Li, Y. Yu, G. J. Ye, Q. Ge, X. Ou, H. Wu, D. Feng, X. H. Chen, and Y. Zhang, *Nat. Nanotechnol.* **9**, 372 (2014).
- [18] H. Yuan, X. Liu, F. Afshinmanesh, W. Li, G. Xu, J. Sun, B. Lian, A. G. Curto, G. Ye, Y. Hikita, Z. Shen, S. C. Zhang, X. Chen, M. Brongersma, H. Y. Hwang, and Y. Cui, *Nat. Nanotechnol.* **10**, 707 (2015).
- [19] R. Xu, J. Yang, Y. Zhu, H. Yan, J. Pei, Y. W. Myint, S. Zhang, and Y. Lu, *Nanoscale* **8**, 129 (2016).
- [20] G. Zhang, A. Chaves, S. Huang, F. Wang, Q. Xing, T. Low, and H. Yan, *Sci. Adv.* **4**, eaap9977 (2018).
- [21] J. Qiao, X. Kong, Z. X. Hu, F. Yang, and W. Ji, *Nat. Commun.* **5**, 4475 (2014).
- [22] G. Zhang, S. Huang, A. Chaves, C. Song, V. O. Özçelik, T. Low, and H. Yan, *Nat. Commun.* **8**, 14071 (2017).
- [23] J. Kim, S. S. Baik, S. H. Ryu, Y. Sohn, S. Park, B.-G. Park, J. Denlinger, Y. Yi, H. J. Choi, and K. S. Kim, *Science* **349**, 723 (2015).
- [24] A. N. Rudenko and M. I. Katsnelson, *Phys. Rev. B* **89**, 201408(R) (2014).
- [25] J. Yang, R. Xu, J. Pei, Y. W. Myint, F. Wang, Z. Wang, S. Zhang, Z. Yu, and Y. Lu, *Light Sci. Appl.* **4**, e312 (2015).
- [26] W. Shan, A. J. Fischer, S. J. Hwang, B. D. Little, R. J. Hauenstein, X. C. Xie, J. J. Song, D. S. Kim, B. Goldenberg, R. Horning, S. Krishnankutty, W. G. Perry, M. D. Bremser, and R. F. Davis, *J. Appl. Phys.* **83**, 455 (1998).
- [27] G. Moody, C. Kavir Dass, K. Hao, C.-H. Chen, L.-J. Li, A. Singh, K. Tran, G. Clark, X. Xu, G. Berghäuser, E. Malic, A. Knorr, and X. Li, *Nat. Commun.* **6**, 8315 (2015).
- [28] A. Favron, E. Gaufrès, F. Fossard, A.-L. Phaneuf-L'Heureux, N. Y.-W. Tang, P. L. Lévesque, A. Loiseau, R. Leonelli, S. Francoeur, and R. Martel, *Nat. Mater.* **14**, 826 (2015).
- [29] See Supplemental Materials at <http://link.aps.org/supplemental/10.1103/PhysRevB.101.235407> for additional figures and tables.
- [30] X. Wang, J. Xu, C. Wang, J. Du, and W. Xie, *Adv. Mater* **23**, 2464 (2011).
- [31] F. Wang, G. Zhang, S. Huang, C. Song, C. Wang, Q. Xing, Y. Lei, and H. Yan, *Phys. Rev. B* **99**, 075427 (2019).
- [32] V. Pareek, J. Madéo, and K. Dani, *Phys. Rev. Lett.* **124**, 057403 (2020).
- [33] L. Wu, J. Wang, J. Lu, D. Liu, N. Yang, H. Huang, P. K. Chu, and X. Yu, *Small* **14**, 1801405 (2018).
- [34] F. Yang, M. Wilkinson, E. J. Austin, and K. P. O'Donnell, *Phys. Rev. Lett.* **70**, 323 (1993).
- [35] Y. Du, C. Ouyang, S. Shi, and M. Lei, *J. Appl. Phys.* **107**, 093718 (2010).
- [36] A. Rudenko, S. Yuan, and M. Katsnelson, *Phys. Rev. B* **92**, 085419 (2015).
- [37] D. A. Prishchenko, V. G. Mazurenko, M. I. Katsnelson, and A. N. Rudenko, *2D Mater.* **4**, 025064 (2017).
- [38] T. Low, R. Roldán, H. Wang, F. Xia, P. Avouris, L. M. Moreno, and F. Guinea, *Phys. Rev. Lett.* **113**, 106802 (2014).
- [39] A. Chaves, T. Low, P. Avouris, D. Çakır, and F. M. Peeters, *Phys. Rev. B* **91**, 155311 (2015).
- [40] R. Schuster, J. Trinckauf, C. Habenicht, M. Knupfer, and B. Büchner, *Phys. Rev. Lett.* **115**, 026404 (2015).
- [41] A. S. Rodin, A. Carvalho, and A. H. Castro Neto, *Phys. Rev. B* **90**, 075429 (2014).
- [42] L. V. Keldysh, *Pis'Ma Zh. Eksp. Teor. Fiz.* **11**, 716 (1979) [*JETP Lett.* **29**, 658 (1979)].
- [43] J. P. Perdew, K. Burke, and M. Ernzerhof, *Phys. Rev. Lett.* **77**, 3865 (1996).
- [44] P. Giannozzi, S. Baroni, N. Bonini, M. Calandra, R. Car, C. Cavazzoni, D. Ceresoli, G. L. Chiarotti, M. Cococcioni, I. Dabo, A. Dal Corso, S. De Gironcoli, S. Fabris, G. Fratesi, R. Gebauer, U. Gerstmann, C. Gougoussis, A. Kokalj, M. Lazzeri, L. Martin-Samos, N. Marzari, F. Mauri, R. Mazzarello, S. Paolini, A. Pasquarello, L. Paulatto, C. Sbraccia, S. Scandolo, G. Sclauzero, A. P. Seitsonen, A. Smogunov, P. Umari, and R. M. Wentzcovitch, *J. Phys. Condens. Matter* **21**, 395502 (2009).
- [45] S. Grimme, J. Antony, S. Ehrlich, and H. Krieg, *J. Chem. Phys.* **132**, 154104 (2010).
- [46] D. Hamann, M. Schlüter, and C. Chiang, *Phys. Rev. Lett.* **43**, 1494 (1979).
- [47] M. S. Hybertsen and S. G. Louie, *Phys. Rev. B* **34**, 5390 (1986).
- [48] M. Rohlfing and S. G. Louie, *Phys. Rev. B* **62**, 4927 (2000).
- [49] D. Y. Qiu, F. H. Da Jornada, and S. G. Louie, *Nano Lett.* **17**, 4706 (2017).
- [50] R. Fei and L. Yang, *Nano Lett.* **14**, 2884 (2014).
- [51] L. Seixas, A. S. Rodin, A. Carvalho, and A. H. Castro Neto, *Phys. Rev. B* **91**, 115437 (2015).